Ceramics International 48 (2022) 1047–1056

Contents lists available at ScienceDirect

Ceramics International

journal homepage: www.elsevier.com/locate/ceramint

The effect of in-situ formed layered hBN on the machinability and mechanical properties of SPS sintered SiC

Zuhal Yılmaz [a,*], Umut Savacı [b], Servet Turan [b], Nuran Ay [b]

[a] Bilecik Seyh Edebali University, SMYO, 11230, Bilecik, Turkey
[b] Eskişehir Technical University, Faculty of Engineering, Department of Materials Science and Engineering, 26555, Eskisehir, Turkey

ARTICLE INFO

Keywords:
hBN
SiC
Machinability
Composite
Electron microscopy

ABSTRACT

In this study, the relationship between machinability, mechanical properties and microstructure of hBN-SiC composites was investigated. Manufacturing of the composites started with the calcination of raw materials at 850 °C for 16 h under a nitrogen atmosphere prior to mixing with 5 wt% of Al_2O_3:Y_2O_3 sintering additives and then powder mixtures were spark plasma sintered at 1850 °C for 17 min by applying 50 MPa pressure. Characterizations of the samples were carried out with FTIR, XRD, SEM and TEM methods. The physical and mechanical properties of the samples were determined with density measurement, Vickers hardness, Young's modulus, three-point bending, fracture toughness and drill test methods. The amount of in-situ formed hBN phase within the sintered composites was calculated by using the Rietveld method. The physical, mechanical and machinability properties of the composite were evaluated according to the calculated amount of hBN. The highest drilling speed during the test was obtained as 34.24 mm/min for the sample containing 29 wt% of hBN. Increasing the drill load from 19.61 N to 49.03 N resulted in 4.33 times increase in the drilling rate. TEM and STEM studies which were carried out for the microstructural investigations showed the internal defects as delamination bands within hBN phase formed during sintering. In addition to these analyses, novel precession electron diffraction method in TEM was utilized for orientation mapping to investigate any possible orientation relationship between SiC and in-situ synthesized hBN phase.

1. Introduction

Silicon carbide (SiC) is one of the most important high temperature structural ceramics due to its high elastic modulus, high strength at high temperatures as well as high thermal and chemical stability. SiC ceramics are also used in a wide range of applications due to their electronic and semi-conductor properties. Even though SiC has superior mechanical properties at high temperatures, it is limited to obtain complex geometries with machining due to the fragile structure of SiC. Therefore, machinability properties for SiC are very important and machining costs are high.

Hexagonal boron nitride (hBN) is an extraordinary material due to its physical and chemical properties such as low elastic modulus, high thermal shock and electrical resistivity, high chemical stability at elevated temperatures as well as high machinability [1–3]. Due to the high machinability of the hBN, it became a filler material for SiC ceramic composites. On the other hand, one of the major disadvantages of the use of hBN particle addition is the decreased fracture toughness of the composite due to the low fracture toughness and delamination of the micron-sized hBN particles [4,5]. Additionally, the homogeneous distribution of SiC and hBN particles cannot be achieved with conventional mixing methods prior to densification [4,7]. Therefore, studies undertaken recently have focused on the production of hBN-SiC composites having homogeneously distributed sub-micron hBN particles to improve machinability, fracture toughness and thermal shock resistance [2,5–8]. In-situ formation of hBN particles within the SiC matrix, during production of the composites, is an alternative approach to overcome a non-homogeneous hBN particle distribution problem while obtaining sub-micron sized hBN particles.

In the literature, there are several different studies presenting that hBN-SiC composites were produced by in-situ synthesis of hBN and SiC particles with reactions of various starting raw materials. In-situ formation of hBN particles within SiC matrix occurs by chemical reactions of; (i) Si_3N_4, B_4C and C [2,3,9,10], (ii) Si_3N_4, B_2O_3 and C under Ar

* Corresponding author.
E-mail addresses: zuhal.guven@bilecik.edu.tr (Z. Yılmaz), umutsavaci@eskisehir.edu.tr (U. Savacı), sturan@eskisehir.edu.tr (S. Turan), nay@eskisehir.edu.tr (N. Ay).

https://doi.org/10.1016/j.ceramint.2021.09.190
Received 18 July 2021; Received in revised form 11 September 2021; Accepted 16 September 2021
Available online 21 September 2021

atmosphere [8], (iii) B_4C and Si under high pressurized nitrogen atmosphere [11], (iv) nitridation of borosilicate glass by using SiO_2, H_3BO_3 and Si and carbothermal reduction in nitrogen atmosphere [6]. In these studies in which SiC and hBN are synthesized together, the main focus is on the in-situ synthesis methodology besides physical and mechanical properties.

Moreover, some studies examine the machinability of the hBN-SiC composite produced with different starting raw materials, production methods and sintering additives [4,5,7,12,13]. In the hBN-SiC nanocomposites that were produced with in-situ hBN formation by using H_3BO_3 and $CO(NH_2)_2$ raw materials, it was observed that in-situ synthesis methodology resulted in homogeneous hBN particle distribution within SiC matrix [4,5,7,12]. With this synthesis methodology, it is also reported that the size of in-situ formed hBN particles may reach below 100 nm [12], and smaller hBN particles in the composite provide high bending strength [4,7] and fracture toughness [4]. Because small particles have reduced the boundaries, inclusions are more likely to occur within the matrix, and borders can easily break through them. Large particles tend to remain within the grain boundaries because they significantly reduce the boundary energy and are difficult to break through the grain boundaries [12]. Because of this reason, decreasing the size of hBN particles within the composite can result in better machinability of the composites. In SiC composites containing 30 wt % hBN, the drilling velocity in the composites with micron-sized hBN and nano-size hBN was measured as 7.8 mm/min and 10.5 mm/min respectively [4], which shows that decreasing the hBN particle size improves the machinability of the composites.

In the literature, the production of SiC-hBN composites has been used generally hot pressing [5,7,12]. This method, since sintering takes place at longer sintering times and higher temperatures, it negatively affects the achievement of mechanical properties expected from materials due to grain growth. SPS method has very high heat efficiency due to the application of high electrical energy to charge between the powder particles and heating of the electrically conductive graphite mold with the high pulsed current. Since the pulse current provides homogeneous heating, materials with homogeneous properties can be obtained in a shorter time [14].

Therefore, the aim of this study is to improve the machinability of the hBN-SiC composite by using in-situ formed submicron hBN particles without losing the superior properties of SiC. For this purpose, the composites were produced by using spark plasma sintering (SPS), the machinability and mechanical properties were measured and microstructural characterizations were carried out.

2. Experimental procedure

The α-SiC (particle size 2 μm, Alfa Aesar, Germany, 99.8%), boric acid (H_3BO_3) (Merck, Germany) and urea ($CO(NH_2)_2$) (Merck, Germany, $\geq$ 99.5%) were used as starting raw materials. The molar ratio of (H_3BO_3):($CO(NH_2)_2$) was 1:3 in composite powder. Powder mixtures were prepared to form 0, 10, 20, 30 and 40 wt% (theoretically) of hBN within the hBN-SiC composite. Starting raw materials that were mixed in a planetary ball mill (Fritsch, Pulverisette) by using silicon nitride (Si_3N_4) balls with 11 mm diameter for 90 min within an ethanol media. Dried powder mixtures were calcined at 850 °C under nitrogen atmosphere for 16 h in a tube furnace (Protherm). Samples were coded as S0, S10, S20, S30 and S40 depending on the hBN content. These calcined powders were mixed with (5 wt%) Al_2O_3 and Y_2O_3 sintering additive mixture with an Al_2O_3:Y_2O_3 weight ratio of 7:3. The powder mixtures were ground by a planetary ball mill with Si_3N_4 balls for 24 h in ethanol and then dried. Afterwards, dried powders were homogenized with planetary ball mill without a liquid medium. The shaping and sintering were done in SPS (HPD-50, FCT GmbH, Germany) at 1850 °C under 50 MPa for 17 min. The heating rate was 100 °C/min up to 1850 °C. The electric current was pulsed periodically with 12 pulses/ms (2 of 12 pulses off as a recovery time). The temperature was increased by controlled electrical current and was measured with an optical pyrometer inside the graphite punches.

X-Ray diffractometer (XRD- Rigaku Rint 2000) was used to determine the crystalline phases of the calcined composite powders and sintered materials. XRD patterns were obtained with Cu-K_α radiation (λ = 1.5418 Å), in the 2θ range of 20–80° with the scan speed of 2°/min at all samples. To determine the presence of BN after calcination on S30 sample, scan range 20–30°(2θ) with scan speed of 0.2°/min was used. Quantitative phase analysis was carried out by using JADE software and Maud program. The microstructure is characterized by means of scanning electron microscopy (SEM, ZEISS SUPRA 50VP) which equipped with an energy dispersive x-ray probe (EDX, Oxford Instruments, UK). Transmission electron microscopy (TEM, JEOL-JEM 2100F) studies were conducted by using field emission TEM equipped with STEM high angle annular dark field (HAADF, Fischione-Model 3000) energy dispersive spectrometer (EDX, JEOL-JED2300T) and precession electron diffraction (PED, Nanomegas) with 0.7° of precession angle.

Density and open porosity were evaluated by Archimedes′ principle. The theoretical density was obtained using the mass fractions and densities. The theoretical SiC and hBN densities were taken as 3.21 g/cm^3 and 2.27 g/cm^3, respectively. Micro-hardness was tested on polished surface by Vickers′ indentation with a load of 10 Kg (EMCO TEST M1C 010). The fracture toughness of the samples was determined from the Vickers indentation method and calculated according to equation (1) [15]. In this equation; E: elastic modulus, c: half-length of surface crack distance, P: load and H_V: Vickers hardness.

$$K_{IC} = 0.018\left(\frac{E}{H_V}\right)^{0.5}\frac{P}{c^{1.5}} \quad (1)$$

The bending strength of the samples was measured with INSTRON 5581 test machine. Sintered samples were cut according to the three-point bending standards (3 mm thickness, 4 mm width and 28 mm length).

Drill tests were carried out by using TOS brand desktop drill and drill velocity was calculated with ratio of drill height (H) to time (t). For this test, a tungsten carbide (WC) drill bit having 2 mm diameter was used and all tests were carried out with a brand new drill bit. The test was carried out at 500 rpm in two different loads (19.6 and 49.03 N) and the test was repeated three times.

3. Results and discussion

3.1. Phase compositions and microstructures

XRD patterns of the S30 sample after calcination at 850 °C are given in Fig. 1. This figure clearly shows that during calcination BN formation starts. BN is in the turbostratic phase, up to 1300 °C [16] and according

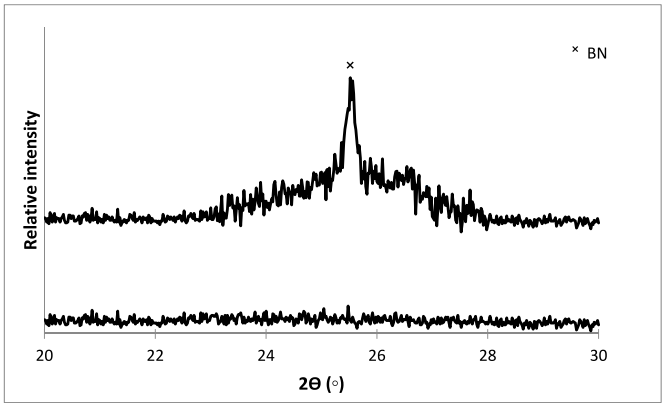

Fig. 1. XRD pattern of S30 sample after calcination at 850 °C (above spectrum was obtained with 0.2°/min scan speed whereas below one obtained with 2°/min scan speed).

to this result, the calcination process results in formation of turbostratic BN (tBN) due to the reaction between boric acid and urea. The formation of BN is also supported by the hBN peaks in the FTIR analysis, which is given in Fig. 2. In the FTIR spectrum, two strong characteristic peaks are located at 1383 and 787 cm^{-1} which could be observed clearly in the sample. The peak at 1383 cm^{-1} can be attributed to the B–N stretching vibrations [17,18]. The peak located at 787 cm^{-1} occurs due to the B–N–B bending vibrations [17] and the other peak located at 829 cm^{-1} is the result of Si–C stretching vibrations [19,20]. The 2342 and 2360 cm^{-1} peaks are attributed to environmental CO_2 gas. Some authors relate this band to atmospheric CO_2 [21,22].

XRD patterns of the sintered samples are given in Fig. 3 and according to these results, the composite samples are composed of hBN (JCPDS PDF No: 034-0421), 4H–SiC (JCPDS PDF No:022-1317) and 6H–SiC (JCPDS PDF No:075-8314) polymorphs. WC contamination was caused by grinding in the tungsten carbide mill during XRD sample preparation. SEM secondary electron images of the fractured surfaces of the sintered samples are given in Fig. 4. The sintering additives in the S0 sample are located between SiC particles. The sample S10 has a very small amount of hBN and hBN particles that are not as easily seen as in other samples. In the hBN formed samples even though the sintering additive phase was not observed between phases, SEM-EDX analysis (given in Fig. 5) showed that Al and Y peaks were present in the spectrum, showing that sintering additives were present in the microstructure but possibly due to their small size, detailed microstructural characterizations need to be carried out with TEM methods.

In these samples, (S)TEM analyses reveal that the sintering additive phase is mostly found not only as grain boundary phase between hBN and SiC but also at the triple junctions of hBN and SiC grains (Figs. 6, 7). STEM-EDX spectra of the liquid phase are given in Fig. 8 (d) and it consists of Si, Y, Al and O elements. In a study by Gao et al., the reason why the glassy phase could not be seen in the samples although the glassy phase was initially added in the BN/Si_3N_4 composite was explained with the high mobility of glass phase on the matrix grain boundary, that prevented it from being entrapped into the moving matrix grains during sintering [23]. Therefore, sintering additive phase is not only present at triple junctions but also distributed between grain boundaries. TEM image of S20 sample in Fig. 6 shows that hBN particles are formed around SiC particles and sintering additive phase surrounds the hBN particles.

In both SEM and TEM images (Figs. 4, 6b and 7b), it can be observed that hBN particles are buckled and delaminated which is believed to be caused by the thermal stresses during SPS [23]. In the TEM images of the hBN particles, it is found that delamination occurs between basal planes as shown in inset image of Fig. 6b. Similar delamination bands were also present in hBN-SiC composite in literature and these delamination bands were identified as kink bands or deformation twins depending on the inclination angle of the delaminated strands [24]. In this study, inclination angles of delaminated strands are formed by the formation of compression/shear stresses during SPS process due to the thermal expansion coefficient differences. The thermal expansion coefficient of 6H–SiC is almost isotropic and reported as 4.2 × 10^{-6} K^{-1} and 4.7 × 10^{-6} K^{-1} between 0 and 423 °C for a and c-axes, respectively. However, the thermal expansion coefficient of hBN is highly anisotropic and reported as 0 K^{-1} for a-axis and 40.5 × 10^{-6} K^{-1} for c-axis at 770 °C [25]. This anisotropic thermal expansion behavior of hBN, causes significant shrinkage along c-axis, which resulted in tension stress along c-axis. However, along a-axis there was no stress due to zero thermal expansion coefficient of hBN during cooling, but there could be tension stress due to the shrinkage of surrounding 6H–SiC particles during cooling from sintering temperature to room temperature. Therefore, net stress becomes a shear stress along c-axis of hBN crystal which might cause delamination. In order to identify the character of the deformation bands, an inclination angle of them within hBN particles was measured and it was found that angles vary between 136° and 163°; however none of them is 139° which is a criteria for deformation twins [25]. Thus, none of delamination bands were characterized as deformation twin. Considering the possibility of kinking of [0001] planes, none of them satisfy the inclination angle relationship requirements. In the light of these findings, delamination bands are identified as deformation bands, which are caused during cooling by strain formation that occurs due to the thermal expansion coefficient mismatch. This thermal expansion coefficient mismatch between hBN and SiC also causes hBN percolation network which can facilitate defect formation at the boundaries [9]. The addition of Al_2O_3–Y_2O_3 sintering additives resulted in the formation of amorphous continuous secondary phase at the hBN-SiC grain boundaries and triple junctions as shown in Fig. 7. The amorphous phase is resulted with a bright contrast in STEM-HAADF images as shown in Fig. 7 due to its chemical composition which consists of high atomic number elements. The chemical composition of amorphous phase consists of Si–O–Al–Y elements and corresponding EDX spectrum is given in Fig. 7d. The thermal expansion mismatch between secondary phase and SiC might also cause residual stress between phases that might result in intergranular fracture [26].

In Fig. 8, TEM and STEM-HAADF images of S40 sample which contains around 29 wt% of hBN are given. According to these images, in

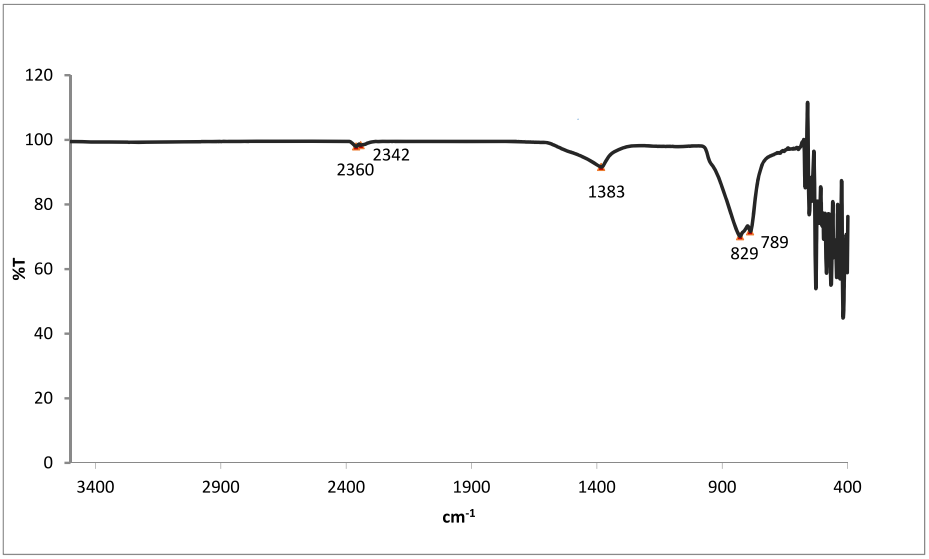

Fig. 2. FTIR spectra of S30 sample after calcination at 850 °C.

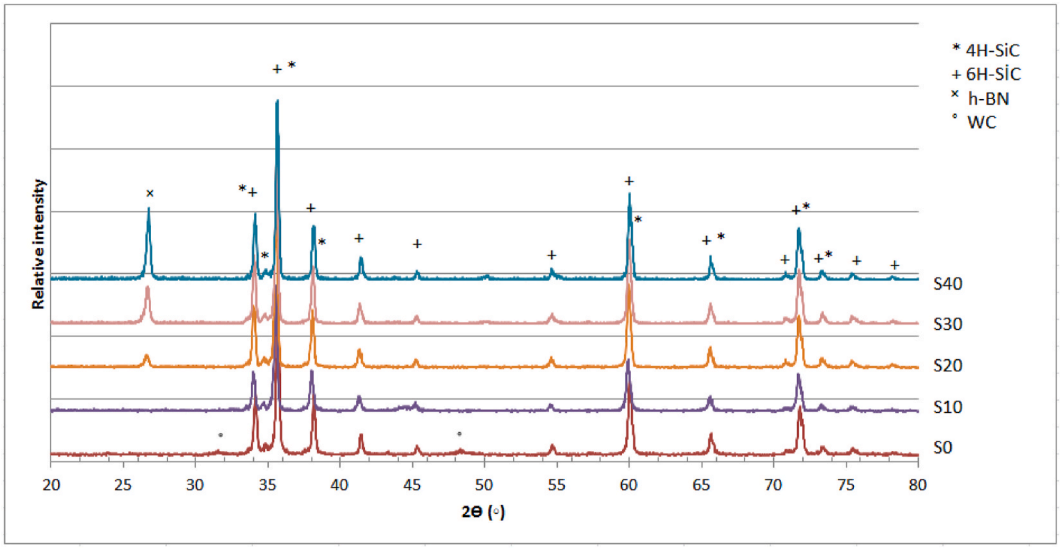

Fig. 3. XRD patterns of S0, S10, S20, S30 and S40 samples that are sintered at 1850 °C.

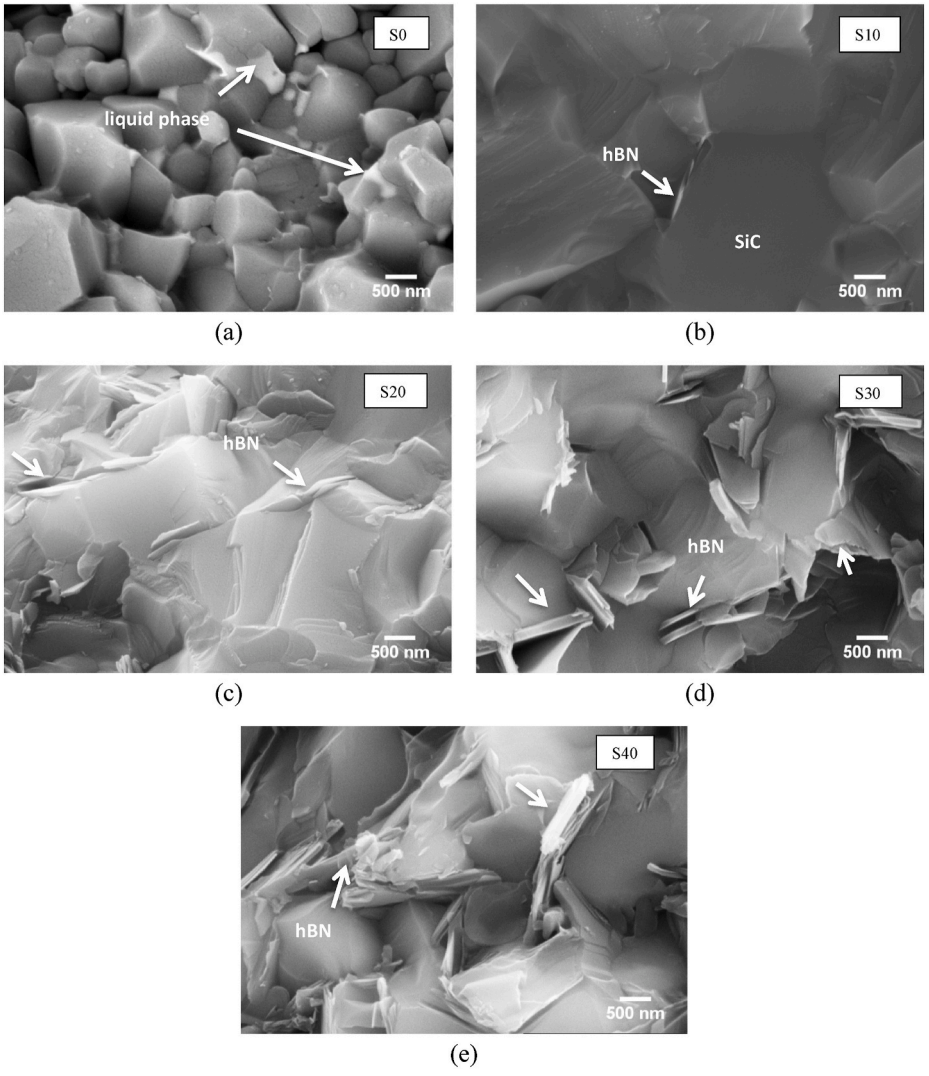

Fig. 4. Fracture surface SEM images of samples, (a) S0, (b) S10, (c) S20, (d) S30 and (e) S40 samples that are sintered at 1850 °C.

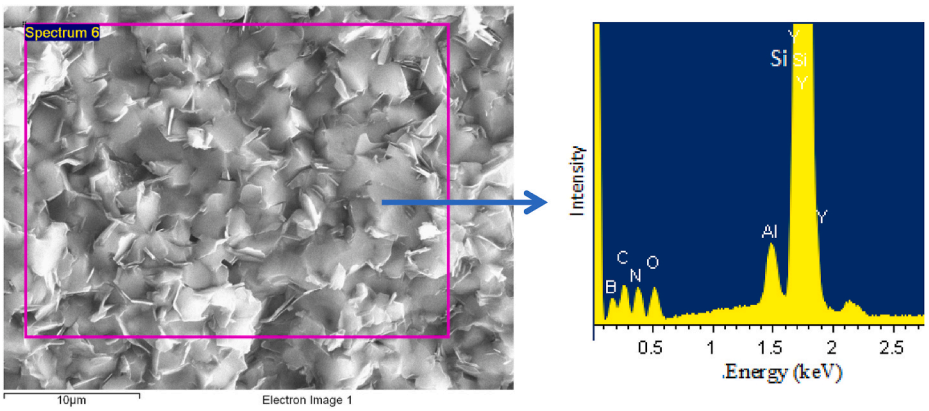

Fig. 5. EDX analysis of the S40 sample that are sintered at 1850 °C.

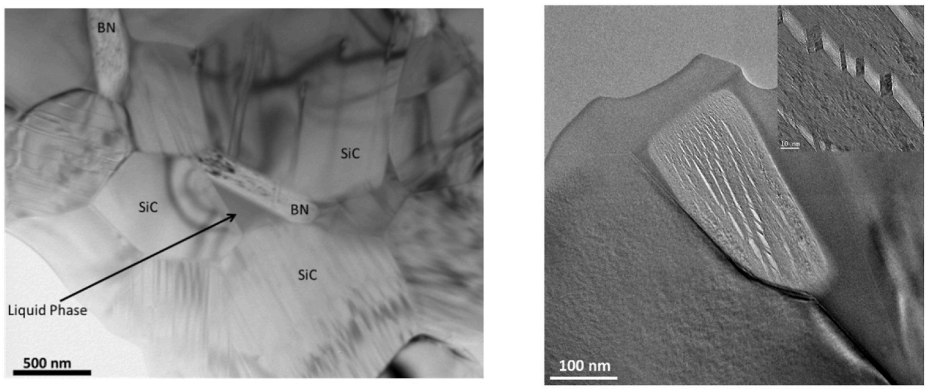

Fig. 6. TEM images of the S20 sintered sample showing (a) general overview and (b) in-situ formed hBN particle. Inset shows the magnified image of delamination inside hBN.

some regions hBN particles completely surround the SiC particles, which is in contrast with S20 sample, and they form a percolation network that affects sintering negatively. In both S20 and S40 samples liquid phases consist of Al, Si, Y and O elements, since Si is not intentionally added to the system as raw material, it is believed that Si source is the passive oxidation layer around SiC particles.

The STEM-HAADF image of S40 sample is given in Fig. 9 and this image shows that carbon regions which surround liquid phase are present in contrast with S20 sample. It is believed that this residual carbon is caused by the excess urea that is used for the in-situ hBN formation.

3.2. Orientation relations between hBN and SiC phases

Composite structures which are produced by in-situ synthesizing methodology can exhibit orientation relation between in-situ synthesized phases with the host structure. Al_2O_3 in Al [27], WC in Co [28], Ti_2AlN in TiB_2 [29] and hBN in SiC [24,30] can be given as examples for orientation relation of in-situ synthesized structures within matrix phase. In the hBN-SiC samples produced with hot isostatic pressing (HIP) at 2100 °C, there was an in-situ synthesis of hBN inside α-SiC samples and conventional electron diffraction studies show that there is an orientation relation between these phases described with $[11\bar{2}0]_{SiC}//[11\bar{2}0]_{hBN}$ and $(0001)_{SiC}//(0001)_{hBN}$ [30]. These orientation relationships represent low energy special grain boundaries which can enhance the mechanical properties. For these reasons, in addition to the conventional TEM methods, composite samples were also investigated for special boundaries with a novel PED technique to search for any specific orientation relation present between SiC and hBN phases. Orientation relation between hBN and SiC is characterized via (0001) and $(11\bar{2}0)$ pole figures in respect to SiC particles and the obtained results are given in Fig. 10; however, in the analyzed particles no specific relationship was found to be present. Therefore, it can be concluded that in-situ hBN formation resulted in randomly oriented hBN particles around SiC particles.

During the orientation mapping of hBN-SiC composites another feature was found within the hBN particles, that is the twist boundary formation between $(0002)_{hBN}$ planes. As shown in Fig. 10 (a) twist boundaries were found as bands (labelled as 1 and 2) with different orientation compared to parent hBN particle and this type of structure can be identified as hBN bicrystal. Twist boundaries are defined with rotation axis between two grains, which is perpendicular to boundary plane, rotation axis and rotation angle θ [31]. Pole figures obtained from orientation maps of twist bands were used to identify twist boundary and its rotation axis. Based on the pole figures, twist boundary plane was found as (0002) plane and rotation axis was [0001] direction. However, rotation angle θ was measured with misorientation angle between twist band and parent hBN particles. Based on these findings hBN bicrystals composed from two hexagonal crystals with (0001) planes parallel to each other as well as [0001] directions but they are rotated with θ angle, thus $(11\bar{2}0)$ as well as $(01\bar{1}0)$ and $(10\bar{1}0)$ planes were no longer parallel to each other as shown in pole figures obtained from hBN particles labelled as 1 and 2 in Fig. 10. Rotation angles around [0001] direction were found between 9.5° and 29° for different hBN bicrystals and the majority of them were higher than 15° which are called as high angle twist boundary.

The coincident site lattice (CSL) theory is used to identify whether

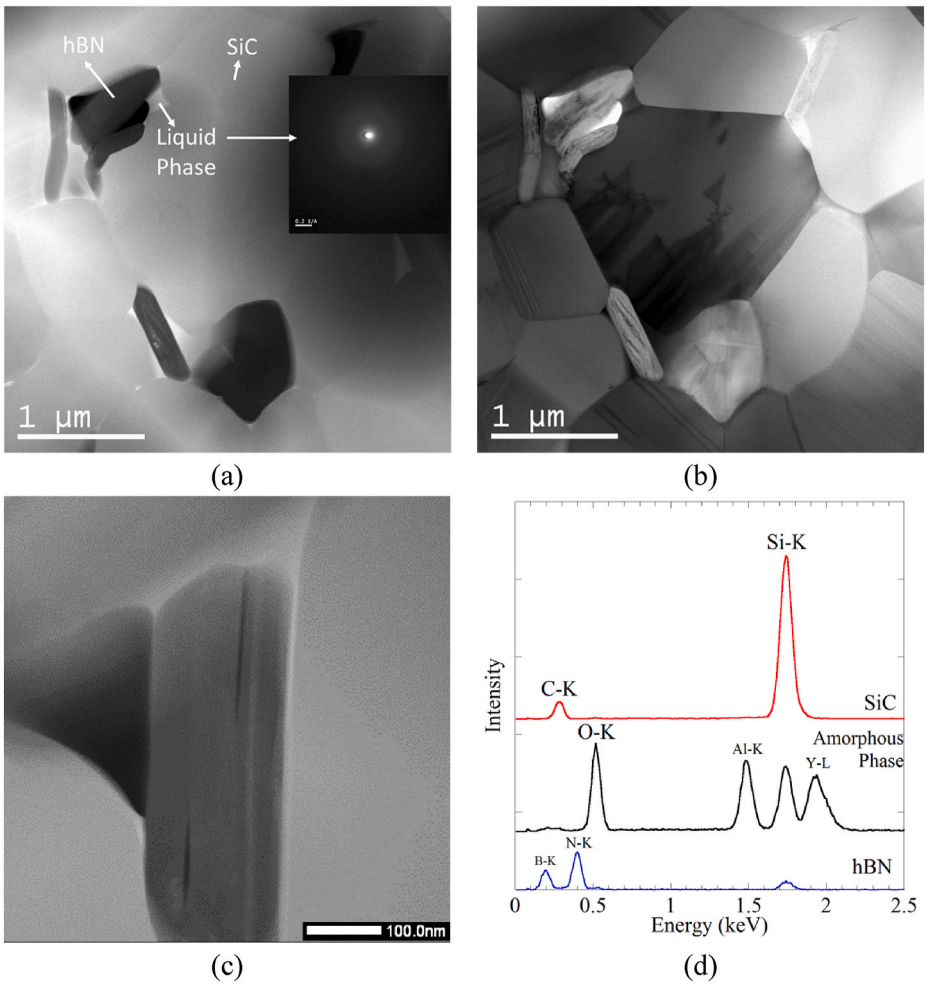

Fig. 7. (a) STEM-HAADF and (b) STEM-BF image of the S20 sintered sample (c) magnified STEM-HAADF image of hBN particle and SiC grain boundary containing amorphous liquid phase and (d) EDX results obtained from hBN, SiC and amorphous phase. (please note that EDX spectrums taken from regions labelled with arrows in (a)).

grain boundaries are special, described by ∑ notation [32], or randomly oriented boundaries. According to CSL theory, some of the twist boundaries having 22°, 28° and 12° of rotation angles are identified as ∑7, ∑13 and ∑19, respectively, for HCP crystals [33–35] and these special boundaries have lowest interfacial energy for rotation around [0001] direction [36]. Other than these special boundaries there are also several random grain boundaries having 24°, 25°, 26° and 27° rotation angles. Based on the presence of special and random twist boundaries, formation of this type of defects within hBN crystal is related to the strains occurred that during cooling due to thermal expansion coefficient mismatch between hBN and SiC, similar to delamination mechanism within hBN particles.

3.3. Quantitative phase analysis

The amounts of in-situ formed hBN phase and SiC polymorphs in the composites were calculated with Rietveld refinement methodology by using Maud software. These measurements, which are given in Table 1, showed that the amounts of in-situ formed hBN phase are lower than the targeted theoretical values. The results showed that not all of the raw materials are involved in the hBN formation reaction according to theoretical calculations. In the process of synthesizing BN, proper amounts of urea help form polyurea to hydrolyze and then release ammonia to react with B_2O_3. The excessive urea accomplishes the solidification process during urea and boric acid reactions and B_2O_3 is packed in the molten products. The packed B_2O_3 cannot come into contact with ammonia and the chemical reaction cannot occur sufficiently. Therefore, the crystallization of BN products decreases [37].

3.4. Physical and mechanical properties of the composites

The physical and mechanical properties of the composites are given in Table 2. According to these results, the bulk density decreased from 3.207 g/cm^3 to 2.797 g/cm^3 with the increasing amount of hBN in the composite. As the hBN contents increase, the percolation network is formed at the grain boundaries [38], this hBN network also prevents obtaining full densification of the composite. Additionally, hBN particles at SiC grain boundaries reduce the densification due to inhibition of the solution-precipitation densification mechanism during sintering [39].

In the sample S10, B and N elements from unreacted excess boric acid and urea caused the formation of point defects within SiC, which increased the diffusivity of Si and C elements. This behavior accelerated the sintering resulted in an increased density as well as hardness of S10 sample. In other samples, the hardness decreased from 23.41 to 6.25 GPa with an increasing amount of hBN. hBN crystal structure is similar to graphite and basal planes of these crystals bonded with weak Van-der Waals forces with each other. As a result of this weak bonding, a fracture can easily occur along basal planes and decrease the hardness of composites as hBN content increases.

The bending strength of samples decreased with an increasing amount of hBN in the composites. The bending strength of monolithic SiC decreased with an addition of 29.10 wt% hBN from 697.7 MPa to

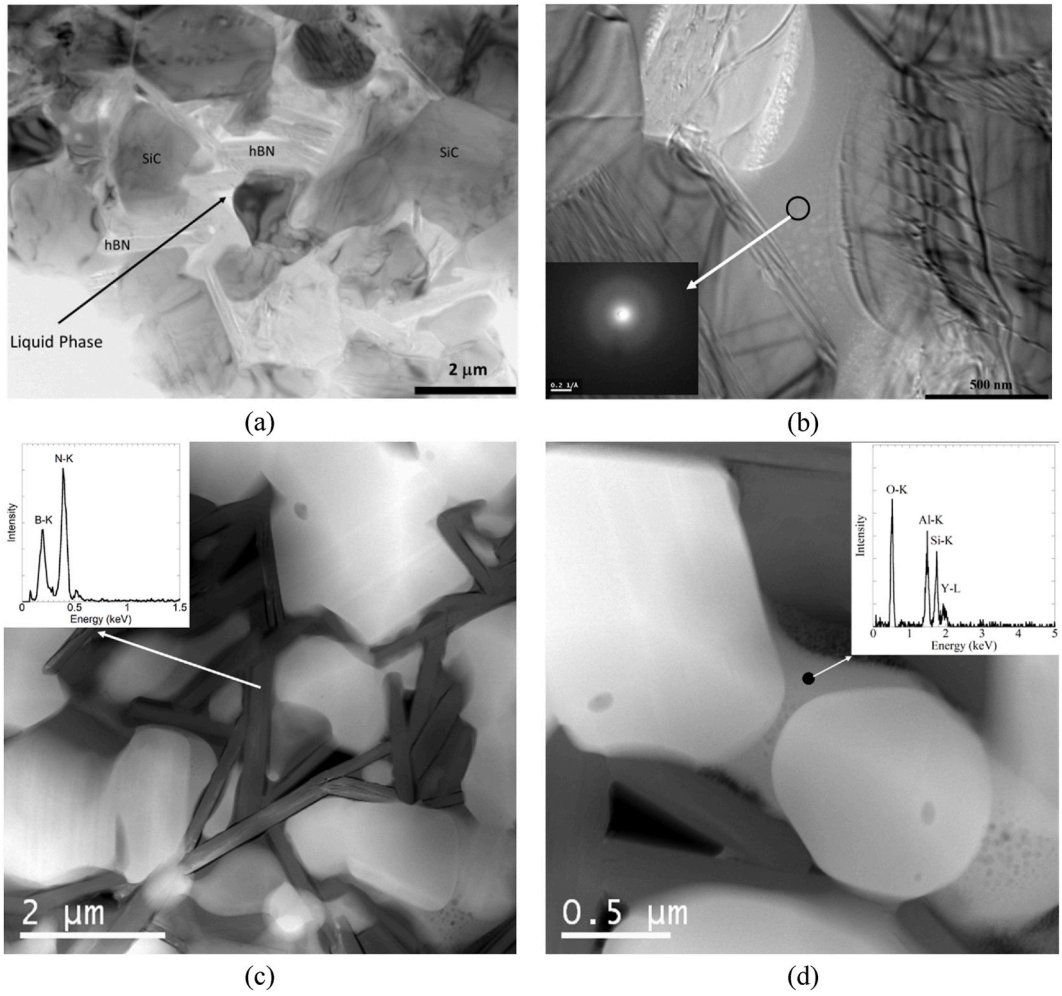

Fig. 8. (a) TEM image showing general overview of the S40 sintered sample, (b) higher magnification TEM image (inset shows the diffraction pattern of amorphous liquid phase), (c, d) STEM-HAADF images and EDX spectrums of hBN and amorphous phase.

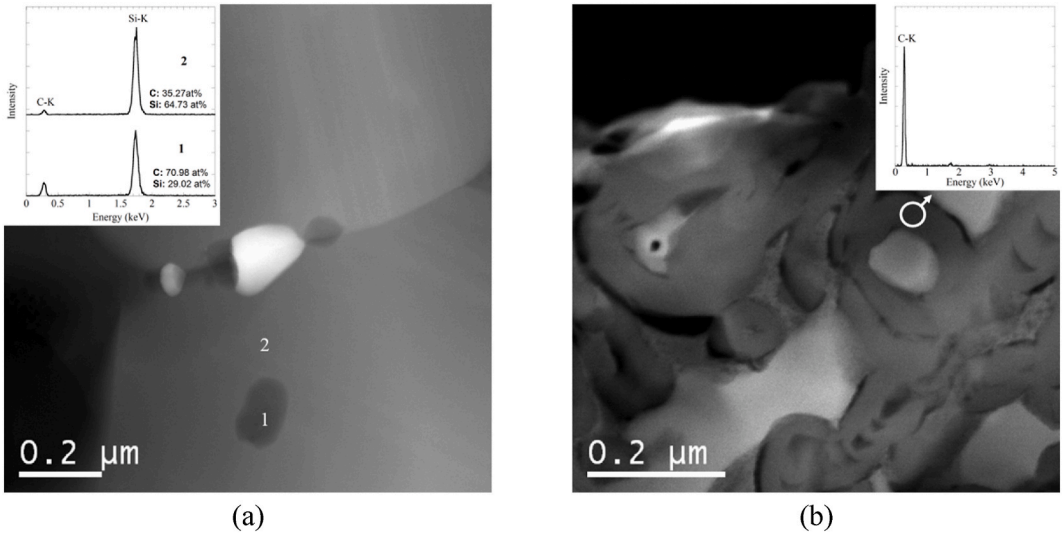

Fig. 9. STEM-HAADF images of the S40 sintered sample showing (a) C-rich region at the surface of SiC and (b) C based secondary phases (insets show the EDX spectra of corresponding regions).

338.2 MPa. According to the studies in the literature, in-situ hBN formation within SiC results in finer and more homogeneous distribution of hBN particles compared with conventional production methods and this may end up with increased strength [3,12]. Compared to monolithic SiC in the hBN-SiC in situ composite study in the literature, it was reported that the strength increased by 9% and 4.4% for 5 vol% and 15 vol% hBN

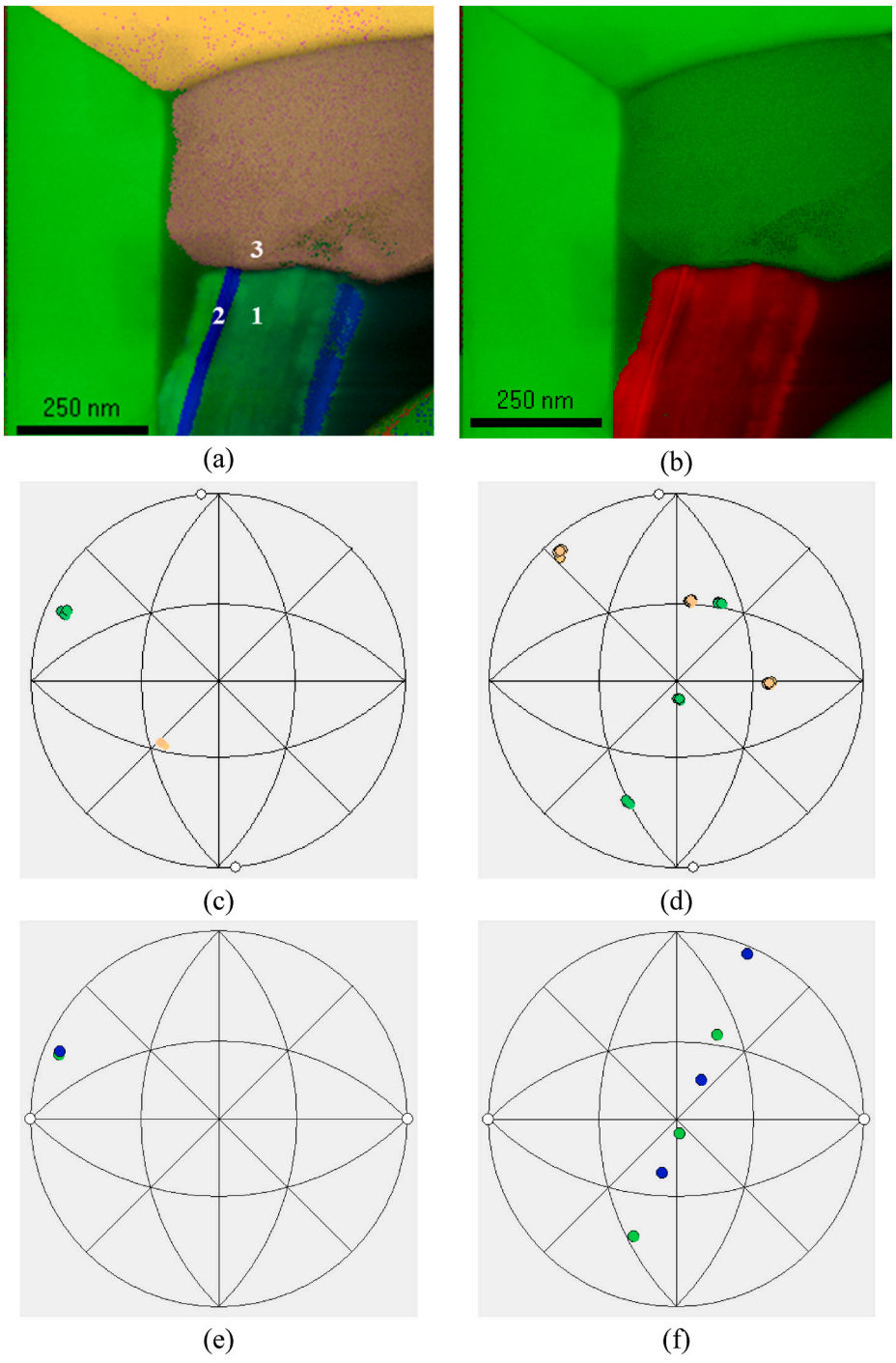

Fig. 10. (a) Orientation and (b) phase (Red: hBN, Green: SiC) maps of the composite,(c) (0001) and (d) (11$\bar{2}$0) pole figures for orientations labelled with 1 and 3 and, (e) (0001) and (f) (11$\bar{2}$0) pole figures for orientations labelled with 1 and 2 (color coded). (11$\bar{2}$0) pole figure shows the misorientation angle between hBN bicrystal as $\sum$7 grain boundary. (For interpretation of the references to color in this figure legend, the reader is referred to the Web version of this article.)

Table 1
Rietveld analysis results of the samples sintered at 1850 °C.

Sample	wt% 6-H SiC	wt% 4-H SiC	Theoretical wt% hBN	Calculated wt% hBN	Experimental % hBN
S0	92.56	7.44	–	–	–
S10	94.94	4.72	10	0.34	3.40
S20	87.74	5.14	20	7.12	35.60
S30	75.28	4.74	30	19.98	66.60
S40	67.01	3.89	40	29.10	72.75

Table 2
Physical and mechanical properties of the hBN-SiC composites.

Sample	Bulk Density (g/cm^3)	Relative Density (%)	Modulus of Elasticity (E) (GPa)	Hardness (GPa)	Bending Strength (MPa)	Fracture Toughness ($MPa.m^{1/2}$)	19.61 N Drilling Rates (mm/min)	49.03 N Drilling Rates (mm/min)
S0	3.207	99.91	241.8	17.94	697.7 ± 98.0	5.17 ± 0.4	0.04	0.09
S10	3.186	99.35	179.9	23.41	530.5 ± 99.6	3.94 ± 0.3	0.07	0.12
S20	3.091	98.35	200.8	18.69	453.4 ± 72.9	4.25 ± 0.3	0.05	0.16
S30	2.914	96.43	154.0	9.85	426.2 ± 29.0	4.20 ± 0.5	0.31	0.52
S40	2.797	95.27	118.7	6.25	338.2 ± 13.8	3.98 ± 0.8	7.91	34.24

containing samples, respectively. In addition, the hBN content was less than 35 vol% while the strength decreased by only about 6%. The formation of hBN particles in SiC, resulted in an increase of strength until the formation of percolation network and as the hBN network grew, an improvement on the strength decreased with the percolation treshold [9]. In this study, the strength was not determined to increase and this can be explained with formation of hBN percolation network and internal stresses. During cooling, because of the thermal expansion mismatch between SiC and hBN particles, thermal strain formation between particles occurred and it resulted in delamination of the hBN particles due to thermal stresses according to the TEM images. In addition to the hBN percolation network, residual stresses caused by the thermal expansion mismatch might resulted in reduced strength of bulk material due to easier advance of crack at grain boundaries [9,10].

Also during TEM analyses, it was found that micron-sized hBN particles were present in microstructure (Fig. 8) and these micron scale hBN particles reduce [7] the bending strength of SiC. In contrast with that, nano-sized in-situ synthesized hBN particles improve fracture strength as well as fracture toughness of SiC up to 15 vol% hBN content; however, higher hBN content resulted in reduction of these properties [6,10]. The bending strength of monolithic SiC, which was hot pressed at 1850 °C, decreased with an addition of 30 vol% hBN from 720 MPa to 275.59 MPa and 426.4 MPa for micro and nanocomposites, respectively [7]. A similar trend was also observed in the samples which were produced with plasma active sintering method [4] as well as hot pressing method [12]. It can be seen that the results obtained in this study are in accordance with the literature. Young's modulus is decreased with increasing hBN content in hBN-SiC composites [6,9,10,12]. Because the hBN has low Young's modulus and reduces the elastic modulus of the composite.

The fracture toughness measurements were made via the Vickers indentation method for SiC monolithic and hBN-SiC composites shown in Table 2. Compared to monolithic SiC, fracture toughness values decrease in composite samples. In situ synthesis of hBN-SiC composites result in a finer microstructure compared to composites produced with conventional powder processing routes, because of this reason in-situ synthesized composites have lower fracture toughness values [4,12]. The fracture toughness of the composites is not only affected by hBN particle size but also sintering additives. In the literature, hBN-SiC samples produced with plasma active sintering method at 1700 °C with 10 wt% Al_2O_3–Y_2O_3 addition were examined. It was reported that when hBN nanoparticles (30 vol%) were chemically synthesized, the fracture toughness of the monolithic SiC decreased from 8.34 MPa $m^{1/2}$ to 4.61 MPa $m^{1/2}$. In the same study, composite sample was produced with conventional mixing of SiC and hBN (30 vol%) starting powders and the fracture toughness value of the micro composite decreased 3.04 MPa $m^{1/2}$ [4]. In contrast with these results, hot pressing at 1850 °C which contains the same amounts of in-situ synthesized hBN and Al_2O_3–Y_2O_3 additive resulted in increase in the fracture toughness of the composite compared to monolithic SiC from 3.13 MPa $m^{1/2}$ to 3.79 MPa $m^{1/2}$ [12]. In S20 and S30 samples compared to the sample S10, the fracture toughness increased slightly with increasing hBN ratio. This behavior is caused by the hBN particles between grains; that is, the hBN, pores and their interfaces cause formation of pull-out, crack bridging, crack deflection and twisted crack path. These mechanisms are responsible for the improvement in the fracture toughness of the composites. However, if the micron-size hBN ratio increases too much, hBN flakes surround the SiC grains and reduce densification and that causes a decrease in fracture toughness. Due to the delamination along basal planes of hBN particles (TEM images shown in Fig. 6b) and weak intergranular bonds, the high possibility of cracking along the hBN layer planes reduces toughness.

Machinability of the samples was measured with drill test with an application of two different loads; 19.61 N and 49.03 N (Table 2). According to the test results drilling rate increases as hBN content increases at all loads. With an increase in applied load, drilling rate increases 4.33 times for S40 sample. The highest machining rate, which is 34.24 mm/min, is obtained in S40 sample that contains 29.10 wt% of hBN. This result, clearly shows that hBN particles work as a solid lubricant during the machining of the composites.

For machining of a sample, applied compressive stresses need to overcome shear stresses. When applied, compressive stresses become greater than minimum fracture stress, fracture and microcracks, related with hBN and pores will be formed if drilling load is lower than the critical value, machining of the material cannot be performed because of the fact that bonding strength at grain boundary is greater than drilling load. Whenever the drilling load becomes greater than grain boundary strength, composite deforms via particles delamination. If drilling load continues to increase microcracks can be linked to form a net-like microcracks zone and improve the drilling rate [40]. The weaker the intergranular bonds, the greater the degree of crack deflection becomes and the intergranular cracking mode relates to the possibility of cracking along the hBN layer planes [41]. The delamination along basal planes of hBN particles, TEM images given in Fig. 6b, might have a significant role during machining. During machining, cracks can easily be formed along basal planes due to weak van der Waals forces between planes, therefore machinability will increase. Additionally, presence of thermal stresses formed due to thermal expansion mismatch between particles might weaken the bonding strength, thus transgranular fracture mode is promoted which may also have a positive effect on the machinability. Another aspect in the machinability of hBN-SiC composites is the semi-plastic behavior of forces between SiC grains and surrounding, dispersed hBN particles [5]. Last but not least, due to layered structure, it is easy to deform hBN particles. In addition to that, as the hBN particle gets smaller, the surface area of the weak phase increases, therefore, machinability can be eased [7,42].

4. Conclusions

In this study, hBN-SiC composites were successfully produced with an in-situ hBN formation approach by using reaction SPS method, and characterizations of physical, mechanical and machinability properties were carried out by using various methods. According to the SEM and TEM images, hBN particles are distributed homogeneously within microstructure due to in-situ formation approach. Rietveld analyses revealed that the content of the hBN in the sintered bodies did not match with expected theoretical values. As the amounts of boric acid and urea increased before sintering, carbon containing regions were found within the sintered composites. The relative density and hardness values of the composites decreased with increasing hBN content. Additionally, higher hBN content resulted in continuous percolation network between SiC

particles which made densification more difficult. Decreased relative density also resulted in reduced fracture toughness. The hardness and Young's modulus of the composites also decreased with increased hBN content. This was due to the delamination of weakly bonded hBN basal planes, however this behavior resulted with increased machinability of the composites. An increase of the drilling load from 19.61 N to 49.03 N resulted in 4.33 times increase of drilling rate in the sample that had the highest hBN ratio.

During microstructural characterizations in TEM, possible orientation relations between in-situ formed hBN and SiC were also investigated; however, no specific orientation relation was found in this composite system, possibly due to the presence of liquid phase between these phases. During these studies, specific orientation relations were found within hBN crystals. Some of the hBN particles contained [0001] twist boundaries that were formed during sintering. Additionally, delamination of the hBN basal planes occurred due to the different thermal expansion coefficients of the constituents which improved the machinability of the samples.

Declaration of competing interest

The authors declare that they have no known competing financial interests or personal relationships that could have appeared to influence the work reported in this paper.

Acknowledgements

The authors would like to thank the financial supports from the Scientific Research Project Commission of Anadolu University (grant numbers: 1406F321 and 1504F168) and one of the authors (U.S.) would like to acknowledge The Scientific and Technological Research Council of Turkey (TUBITAK) Directorate of Science Fellowships and Grant Programmes (BİDEB) 2211 National Ph.D scholarship programme.

References

[1] Y. Kodera, et al., Consolidation of SiC/BN composite through MA-SPS method, J. Mater. Sci. 43 (2008) 6422–6428.
[2] G.-J. Zhang, et al., Reaction mechanism and microstructure development of strain tolerant in situ SiC–BN composites, Acta Mater. 49 (2000) 77–82.
[3] G.J. Zhang, T. Ohji, In situ reaction synthesis of silicon carbide–boron nitride composites, J. Am. Ceram. Soc. 84 (2001) 1475–1479.
[4] H.Y. Jin, et al., Study of machinable silicon carbide–boron nitride ceramic composites, Mater. Sci. Eng. (2008) 214–217.
[5] T. Kusunose, et al., Contact damage of silicon carbide/boron nitride nanocomposites, J. Am. Ceram. Soc. Japan. 90 (2007) 3341–3344.
[6] T. Kusunose, et al., Synthesis of SiC/BN nanocomposite powders by carbothermal reduction and nitridation of borosilicate glass, and the properties of their sintered composites, Nanotechnology 19 (2008) 275603.
[7] H. Jin, et al., Fabrication and properties of machinable SiC/h-BN Nano-composites, J. Ceram. Process. Res. 9 (6) (2008) 630–633.
[8] G.-J. Zhang, et al., In situ reaction synthesis of silicon carbide–boron nitride composite from silicon nitride–boron oxide–carbon, J. Am. Ceram. Soc. 85 (2002) 2858–2860.
[9] G.J. Zhang, T. Ohji, Effect of BN content on elastic modulus and bending strength of SiC–BN in situ composites, Mater. Res. Soc. 15 (2000) 1876–1880.
[10] Z.H. Yang, et al., Thermal shock resistance of in situ formed SiC–BN composites, Mater. Chem. Phys. 107 (2007) 476–479.
[11] Y.T. Zheng, et al., Microstructure and mechanical properties of h-BN–SiC ceramic composites prepared by in situ combustion synthesis, Mater. Sci. Eng. 540 (2012) 102–106.
[12] X. Wang, et al., Fabrication of machinable silicon carbide–boron nitride ceramic nanocomposites, J. Am. Ceram. Soc. 87 (2004) 565–570.
[13] X. Wang, et al., Preparation of SiC/BN nanocomposite powders by chemical processing, Mater. Lett. 58 (2004) 1419–1423.
[14] Z.H. Zhang, et al., The sintering mechanism in spark plasma sintering – proof of the occurrence of spark discharge, s.l. : Scripta Mater. 81 (2014) 56–59.
[15] B.R. Lawn, et al., Elastic/plastic indentation damage in ceramics: the median/radial crack system, J. Am. Ceram. Soc. 63 (1980) 574–580.
[16] M. Hubácek, et al., High-temperature behaviour of hexagonal boron nitride, Thermochim. Acta 282–283 (1996) 359–367.
[17] D. Besisa, et al., Low temperature synthesis of nano-crystalline h-boron nitride from boric acid/urea precursors, J. Ceram. Process. Res. 17 (2016) 1219–1225.
[18] L.J. Berchmans, et al., Synthesis of nanocrystalline boron nitride by combustion process, Int. J. Self-Propag. High-Temp. Synth. 18 (1) (2009) 34–37.
[19] F. Shariatmadar Tehrani, et al., Pressure dependent structural and optical properties of silicon carbide thin films deposited by hot wire chemical vapor deposition from pure silane and methane gases, J. Mater. Sci. Mater. Electron. 24 (4) (2013) 1361–1368.
[20] L. Saravanan, et al., Surface chemical studies on SiC suspension in the presence of chitosan, Ceram. Int. 32 (6) (2006) 637–646.
[21] M.T. Hernández, M. González, Synthesis of resins as alpha-alumina precursors by the Pechini method using microwave and infrared heating, J. Eur. Ceram. Soc. 22 (16) (2002) 2861–2868.
[22] A. Oancea, et al., Laboratory infrared reflection spectrum of carbon dioxide clathrate hydrates for astrophysical remote sensing applications, Icarus 221 (2) (2012) 900–910.
[23] L. Gao, et al., *BN/Si_3N_4 nanocomposite with high strength and good machinability*, Mater. Sci. Eng., A 415 (1) (2006) 145–148.
[24] S. Turan, K.M. Knowles, Microstructural characterisation of silicon nitride- silicon carbide particulate composites, in: Churchill College, University of Cambridge, Cambridge, 1995.
[25] S. Turan, K.M. Knowles, High resolution transmission electron microscopy of the planar defect structure of hexagonal boron nitride, Phys. Status Solidi 150 (1) (1995) 227–237.
[26] J.H. She, K. Ueno, Densification behavior and mechanical properties of pressureless-sintered silicon carbide ceramics with alumina and yttria additions, Mater. Chem. Phys. 59 (2) (1999) 139–142.
[27] H. Wang, et al., In situ fabrication and microstructure of Al2O3 particles reinforced aluminum matrix composites, Mater. Sci. Eng., A 527 (12) (2010) 2881–2885.
[28] X. Wang, et al., Orientation relationship in WC-Co composite nanoparticles synthesized by in situ reactions, Nanotechnology 26 (14) (2015) 145705.
[29] G. Zhao, et al., In-situ synthesis, microstructure and properties of Ti2AlN/TiB2 composite, Int. J. Mater. Res. 108 (2) (2016) 133–138.
[30] S. Turan, K.M. Knowles, Effect of boron nitride on the phase stability and phase transformations in silicon carbide, J. Am. Ceram. Soc. 79 (12) (1996) 3325–3328.
[31] P. Louisette, Grain Boundaries: from Theory to Engineering. Springer Series in Materials Science, Springer, Netherlands, 2013.
[32] V. Randle, The coincidence site lattice and the 'sigma enigma', Mater. Char. 47 (5) (2001) 411–416.
[33] H. Schmid, M. Rühle, Structure of special grain boundaries in SiAlON ceramics, J. Mater. Sci. 19 (2) (1984) 615–628.
[34] X. Liu, J. Wang, Low-energy, mobile grain boundaries in magnesium, Sci. Rep. 6 (2016) 21393.
[35] J. Shimomura, et al., Electron microscopy of hexagonal boron nitride powder, J. Mater. Sci. 30 (12) (1995) 3193–3199.
[36] Y. Wang, et al., Coincidence-site-lattice twist boundaries in bicrystalline α-Fe2O3 nanoblades, J. Phys. Chem. C 118 (11) (2014) 5796–5801.
[37] Y. Mu, et al., Influence of dip-coated boronnitride interphase on mechanical and dielectric properties of SiCf/SiC composites, Mater. Sci. Eng. 578 (2013) 72–79.
[38] K.J. Kim, et al., Electrical and thermal properties of silicon carbide–boron nitride composites prepared without sintering additives, J. Eur. Ceram. Soc. 35 (16) (2015) 4423–4429.
[39] A. Motealleh, *Effect of hexagonal-BN additions on the sliding-wear resistance offine-grained alpha-SiC densified with $Y_3Al_5O_{12}$ liquid phase by spark-plasma sintering*, s.l. : J. Eur. Ceram. Soc. 34 (2014) 565–574.
[40] Z. Shi, et al., *Machinability, deformation, and cracks behavior of pressureless-sintered Al_2O_3/h-BN composites: role of weak boundary phases*, J. Mater. Sci. 44 (6) (2009) 1580–1587.
[41] W.-S. Cho, et al., Effects of h-BN additive on the microstructure and mechanical properties of AlN-based machinable ceramics, Mater. Sci. Eng. 418 (2006) 61–67.
[42] Z. Shi, et al., *Effects of weak boundary phases (WBP) on the microstructure and mechanical properties of pressureless sintered Al_2O_3/h-BN machinable composites*, Mater. Sci. Eng. 492 (1) (2008) 29–34.